

一般セッション(口頭講演) | 11 超伝導: 11.1 基礎物性

📅 2024年9月17日(火) 9:00 ~ 12:00 📍 C31 (ホテル日航新潟 3F)

**[17a-C31-1~11] 11.1 基礎物性**

荻野 拓(産総研)、畑野 敬史(名大)

9:00 ~ 9:15

[17a-C31-1]

2 段階放電プラズマ焼結を用いたK ドープBaFe<sub>2</sub>As<sub>2</sub> 多結晶バルクの臨界電流特性○石渡 翔大<sup>1</sup>、霜山 郁弥<sup>1</sup>、Ayukaryana Nur Rahmawati<sup>1</sup>、山本 明保<sup>1</sup> (1.農工大)

◆ 奨励賞エントリー

9:15 ~ 9:30

[17a-C31-2]

鉄系超伝導体(Ba,K)Fe<sub>2</sub>As<sub>2</sub>単一人工粒界の作製○(D)秦 東益<sup>1</sup>、郭 子萌<sup>2</sup>、Tarantini Chiara<sup>3</sup>、波多 聡<sup>2</sup>、内藤 方夫<sup>1</sup>、山本 明保<sup>1</sup> (1.農工大工、2.九大、3.米国国立強磁場研)

9:30 ~ 9:45

[17a-C31-3]

MBE法による電子ドープニッケル酸化物の作製

○香田 匡貴<sup>1</sup>、納 謙吾<sup>1</sup>、迫田 将仁<sup>1</sup>、下田 周平<sup>2</sup>、市村 晃一<sup>1</sup> (1.北大工、2.北大触研)

◆ 奨励賞エントリー

9:45 ~ 10:00

[17a-C31-4]

Nd:YAGレーザーを用いたPLD 法によるニッケル酸化物薄膜の作製とトポケミカル還元効果

○(M1)森田 航太<sup>1</sup>、山下 琉斗<sup>1</sup>、土橋 礼奈<sup>1</sup>、岡部 博幸<sup>2,3</sup>、中村 惇平<sup>3</sup>、桑原 英樹<sup>1</sup>、門野 良典<sup>3</sup>、足立 匡<sup>1</sup> (1.上智大理工、2.東北大金研、3.KEK 物構研)

◆ 奨励賞エントリー

10:00 ~ 10:15

[17a-C31-5]

超伝導候補新規物質Sr<sub>3</sub>Ni<sub>2</sub>O<sub>5</sub>Cl<sub>2</sub>の高圧合成と物性評価○(D)山根 和樹<sup>1,2</sup>、足立 伸太郎<sup>3</sup>、松本 凌<sup>1</sup>、寺嶋 健成<sup>1</sup>、櫻井 裕也<sup>1</sup>、高野 義彦<sup>1,2</sup> (1.物材機構、2.筑波大、3.KUAS)

10:15 ~ 10:30

[17a-C31-6]

高圧合成・構造解析・物性測定機能付きDACを用いたT<sub>c</sub> = 20 K級新規超伝導体の発見○松本 凌<sup>1</sup>、山根 和樹<sup>1,2</sup>、寺嶋 健成<sup>1</sup>、新名 亨<sup>3</sup>、入船 徹男<sup>3</sup>、櫻井 裕也<sup>1</sup>、高野 義彦<sup>1,2</sup> (1.NIMS、2.筑波大、3.愛媛大)

◆ 奨励賞エントリー ◆ 英語発表

10:45 ~ 11:00

[17a-C31-7]

Development of automatic synthesis system for superconducting alloys

○(D)WeiSheng Wang<sup>1,2</sup>、Kensei Terashima<sup>1</sup>、Yoshihiko Takano<sup>1,2</sup> (1.NIMS、2.Univ. of Tsukuba)

◆ 奨励賞エントリー

11:00 ~ 11:15

[17a-C31-8]

 $(Y_{1-x}Dy_x)Ba_2Cu_3O_y$ の二軸磁場配向挙動の樹脂硬化時間依存性○(M1C)福山 風人<sup>1</sup>、アリ ワリド<sup>1</sup>、足立 伸太郎<sup>1</sup>、木村 史子<sup>1</sup>、堀井 滋<sup>1</sup> (1.京都先端科学大工)

◆ 奨励賞エントリー ◆ 英語発表

11:15 ~ 11:30

[17a-C31-9]

Relationship between tri-axial orientation degrees and magnetic field strength of MRF on  $(Y_{1-x}Dy_x)_{124}$  with various tri-axial magnetic anisotropies.○(M1)Pamoda Piyumali Kahagalla<sup>1</sup>, Shintaro Adachi<sup>1</sup>, Fumiko Kimura<sup>1</sup>, Ataru Ichinose<sup>2</sup>, Shigeru Horii<sup>1</sup> (1.KUAS, 2.CRIEPI)

11:30 ~ 11:45

[17a-C31-10]

試料搬送型の変調回転磁場印加による $REBa_2Cu_3O_y$ 磁場配向の検討○足立 伸太郎<sup>1</sup>、木村 史子<sup>1</sup>、堀井 滋<sup>1</sup> (1.京都先端科学大・工)

11:45 ~ 12:00

[17a-C31-11]

首振り回転磁場下における $REBa_2Cu_3O_7$ 粉末( $RE=Y, Er$ )の配向度と首振り角度の関係○堀井 滋<sup>1</sup>、野津 乃祐<sup>2</sup>、土井 俊哉<sup>2</sup> (1.京都先端科学大・工、2.京大院エネ科)

## 2 段階放電プラズマ焼結を用いた K ドープ BaFe<sub>2</sub>As<sub>2</sub> 多結晶バルクの 臨界電流特性

Critical current characteristics of K-doped BaFe<sub>2</sub>As<sub>2</sub> polycrystalline bulks using  
two-step spark plasma sintering

東京農工大学<sup>1</sup> °石渡 翔大<sup>1</sup>, 霜山 郁弥<sup>1</sup>, Nur Rahmawati Ayukaryana<sup>1</sup>, 山本 明保<sup>1</sup>

Tokyo Univ. of Agri. and Tech.<sup>1</sup> °Shota Ishiwata<sup>1</sup>, Fumiya Shimoyama<sup>1</sup>,

Nur Rahmawati Ayukaryana<sup>1</sup>, Akiyasu Yamamoto<sup>1</sup>

E-mail: s230587z@st.go.tuat.ac.jp

鉄系高温超伝導体[1]の1種であるBaFe<sub>2</sub>As<sub>2</sub>(Ba122)は元素置換により超伝導が発現する。Baサイトの一部をKで置換したKドープBa122は高い臨界温度( $T_c=38$  K[2])と上部臨界磁場( $H_{c2}>50$  T[3])を持ち、強力磁石等への応用が期待されている。最近、我々は放電プラズマ焼結(SPS)法を用いたKドープBa122バルクにおいて、 $1\times 10^5$  A/cm<sup>2</sup>を超えるランダム方位の多結晶では高い臨界電流密度( $J_c$ )を達成した[4~5]。一方で、薄膜では $1\times 10^6$  A/cm<sup>2</sup>以上の高い $J_c$ [6]が報告されている。本研究では、2段階SPS[7~9]を用いて熱処理条件による配向度と $J_c$ への影響を評価した。Ar雰囲気グローブボックス内で仕込組成Ba<sub>0.6</sub>K<sub>0.4</sub>Fe<sub>2</sub>As<sub>2</sub>となるように単体金属を秤量し、高エネルギー混合[4]することでKドープBa122前駆体を作製した。その後、SPS法によりΦ10 mmのバルクを作製した(1<sup>st</sup> step SPS)後、Φ15 mmの型に1<sup>st</sup> step SPSバルクを充填し再度SPS法によりバルクを得た(2<sup>nd</sup> step SPS)。Fig. 1に700°Cと800°Cで作製した2<sup>nd</sup> step SPSバルク小片の磁化測定による磁化ヒステリシスループを、挿入図に $J_c$ の外部磁場依存性を示す。700°C試料ではバ

ルクXRDにより明らかな配向を確認でき、 $J_c$ は $1.4\times 10^5$  A/cm<sup>2</sup> (SF, 5 K)と高い値を示した。一方で、800°C試料では700°C試料よりも強い配向を示したにもかかわらず $J_c$ は低下した。Fig. 1より800°C試料では磁化ヒステリシスループの0 T付近に2つのピークが存在し、Hecherらのモデル[10]によると粒間電流と粒内電流が混在する中粒径の磁化挙動を示している。800°C試料では比較的大きい粒径の影響で磁化が制限された可能性があり、700°C試料では粒径を抑えて配向したことで高 $J_c$ が得られたことが考えられる。

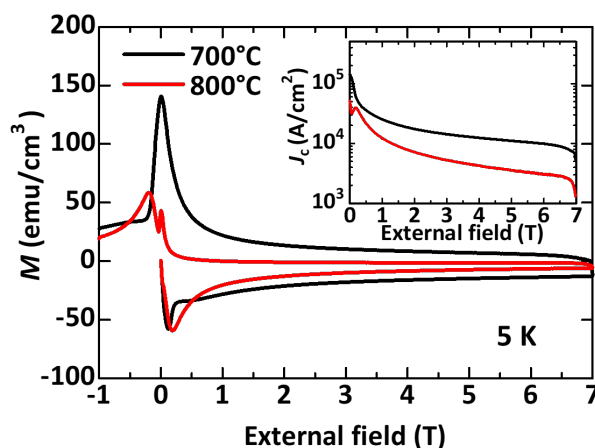


Fig. 1 Magnetic hysteresis loops.  
The inset shows external field dependence of  $J_c$ .

[1] Y. Kamihara *et al.*, *J. Am. Chem. Soc.* **130**, 11 (2008). [2] M. Rotter *et al.*, *Phys. Rev. Lett.* **101**, 107006 (2008). [3] C. Tarantini *et al.*, *Phys. Rev. B* **84**, 184522 (2011). [4] S. Tokuta *et al.*, *iScience* **25**, 103992 (2022). [5] A. Yamamoto *et al.*, *NPG Asia Mater.* **16**, 29 (2024). [6] D. Qin *et al.*, *Supercond. Sci. Technol.* **35**, 09LT01 (2022). [7] S. Ishiwata *et al.*, JSAP Autumn Meeting 20p-B202-11 (2023). [8] J. G. Noudem *et al.*, *Scr. Mater.* **66**, 258 (2012). [9] S. Ishida *et al.*, *J. Alloys Compd.* **961**, 171093 (2023). [10] J. Hecher *et al.*, *Supercond. Sci. Technol.* **29**, 025004 (2016).

## 鉄系超伝導体(Ba,K)Fe<sub>2</sub>As<sub>2</sub> 単一人工粒界の作製

### Artificial grain boundary of the Fe-based superconductor (Ba,K)Fe<sub>2</sub>As<sub>2</sub>

農工大<sup>1</sup>, 九大<sup>2</sup>, 米国国立強磁場研<sup>3</sup> ○(D3) 秦 東益<sup>1</sup>, 郭 子萌<sup>2</sup>, Chiara Tarantini<sup>3</sup>, 波多 聰<sup>2</sup>,  
内藤 方夫<sup>1</sup>, 山本 明保<sup>1</sup>

Tokyo Univ. Agricul. and Technol.<sup>1</sup>, Kyushu Univ.<sup>2</sup>, NHMFL<sup>3</sup>, ○Dongyi Qin<sup>1</sup>, Zimeng Guo<sup>2</sup>,  
Chiara Tarantini<sup>3</sup>, Satoshi Hata<sup>2</sup>, Michio Naito<sup>1</sup>, Akiyasu Yamamoto<sup>1</sup>

E-mail: s210351w@st.go.tuat.ac.jp

鉄系超伝導体<sup>[1]</sup>は銅酸化物系超伝導体に次ぐ高い臨界温度を有しており、電磁的異方性が小さいことや結晶粒界の方位差が臨界電流密度 ( $J_c$ ) に及ぼす影響が小さい<sup>[2]</sup>ことから、配向化を必要としない多結晶体としての応用が期待されている。鉄系超伝導体のなかで、(Ba,K)Fe<sub>2</sub>As<sub>2</sub>は 38 K の比較的高い臨界温度と 50 T を超える上部臨界磁場を有していることから、強磁場への応用に向けた研究が盛んに進められている。

本研究では鉄系超伝導体の結晶粒界特性の解明に向けて、(Ba,K)Fe<sub>2</sub>As<sub>2</sub> エピタキシャル薄膜を [001]チルト粒界 SrTiO<sub>3</sub> バイクリスタル基板上に成膜することを目的とした。薄膜作製は分子線エピタキシー法を用いて行った<sup>[3]</sup>。基板には、表面エッチングを施していない SrTiO<sub>3</sub>(001)基板を用いた。まず、これまでに報告の無い SrTiO<sub>3</sub> 基板上に(Ba,K)Fe<sub>2</sub>As<sub>2</sub>を成膜するため、単結晶基板上に 20 nm 程度の BaFe<sub>2</sub>As<sub>2</sub>をバッファ層として導入した。作製した(Ba,K)Fe<sub>2</sub>As<sub>2</sub> 薄膜は、X 線回折パターンにおいて鋭い  $c$  軸配向性と面内四回対称性がみられたことから、エピタキシャル薄膜であると判断した。(008)面のロッキングカーブ半値幅と(103)面の $\phi$ スキンの半値幅はそれぞれ 1.05°と 1.4°であり、試料の結晶性が高いことが示唆された。試料は 38.4 K で鋭い超伝導転移を示し、10 MA/cm<sup>2</sup>を上回る非常に高い  $J_c$ が得られた。同様の方法で、接合角が 24°, 30°, 36.8°の SrTiO<sub>3</sub> バイクリスタル基板上に薄膜を作製し、その結晶構造を調べた。30°以上の高角粒界含め、いずれの接合角のバイクリスタル基板上にも基板の粒界角を反映しながら、エピタキシャル成長していることが確認された (図 1)。また、バイクリスタル基板上に成膜した(Ba,K)Fe<sub>2</sub>As<sub>2</sub> の(103)面の $\phi$ スキンの半値幅は 1°未満であり、Ba(Fe,Co)<sub>2</sub>As<sub>2</sub><sup>[4]</sup>と同等の結晶性の単一人工粒界を得ることに成功した。

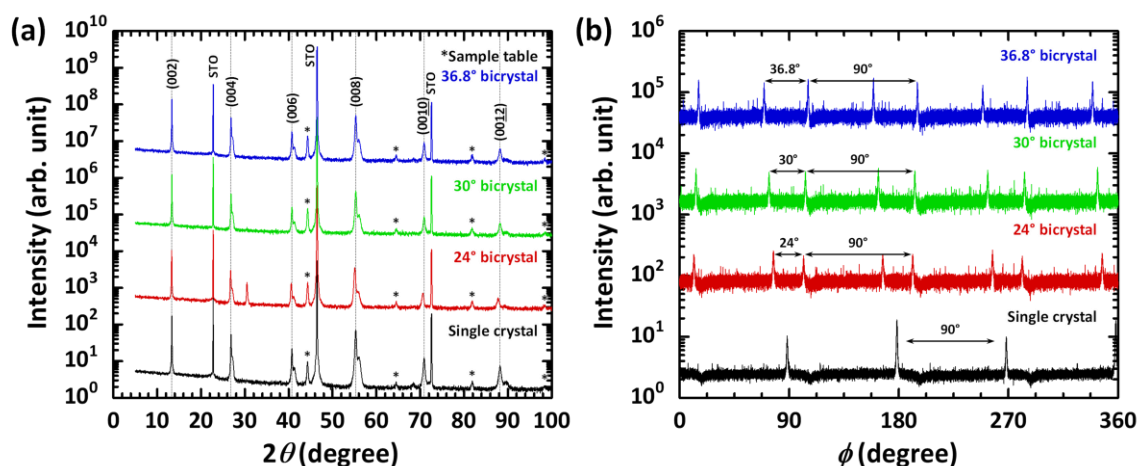


Figure 1. (a)  $2\theta/\omega$ -scan and (b) (103)  $\phi$ -scan of the (Ba,K)Fe<sub>2</sub>As<sub>2</sub> epitaxial thin films on BaFe<sub>2</sub>As<sub>2</sub>-buffered SrTiO<sub>3</sub>(001) single crystal substrate, [001]-tilt-type bicrystalline substrates with a misorientation angle of 24°, 30°, and 36.8°.

#### References

- [1] Y. Kamihara *et al.*, *J. Am. Chem. Soc.* **130**, 3296 (2008). [3] D. Qin *et al.*, *Supercond. Sci. Technol.* **35**, 09LT01 (2022).  
[2] K. Katase *et al.*, *Nat. Commun.* **2**, 409 (2011). [4] K. Iida *et al.*, *Phys. Procedia* **45**, 189 (2013).

## MBE 法による電子ドーピングニッケル酸化物の作製

### Synthesis of electron doped nickel oxide by MBE method

北大工、北大触研<sup>A</sup> ○(M2) 香田 匡貴、(B) 納 謙吾、迫田 将仁、下田 周平<sup>A</sup>、市村 晃一

*Dept. of Appl. Phys. Hokkaido Univ., Lab. of Cat. Hokkaido Univ.*

○Masaki Koda, Kengo Osame, Masahito Sakoda, Shuhei Shimoda, Koichi Ichimura

E-mail: kohda.masaki.e5@elms.hokudai.ac.jp

近年発見された常圧ニッケル酸化物超伝導体[1]は、ペロブスカイト構造をトポケミカル還元して得られる無限層構造である。2次元的な電子構造など銅酸化物超伝導体との共通点もあるが、超伝導相は正孔ドーピング方向に限られており、電子ドーピング方向の相は興味の対象である。

私たちは、ニッケル酸化物内の3価希土類元素Laを4価希土類元素Ceで置換することによって、電子ドーピング方向の相探索を行った(Ceはペロブスカイト構造 $\text{CeNiO}_3$ にて4価となることをX線光電子分光法で確認)。分子線エピタキシー(MBE)法による成膜と $\text{CaH}_2$ 粉末を用いた還元により、様々なドーピング量の無限層構造 $\text{La}_{1-x}\text{Ce}_x\text{NiO}_2$ を作製した。元素比率の評価として、成膜時の水晶振動子(X-tal)での分子線レート制御とエネルギー分散X線分光法(EDS)の測定結果を照らし合わせた (Fig.1)。各試料のデータからX-talで制御したCeレートに対する作製した膜のドーピング量が比例していることがわかり、狙い通りのCeドーピングに成功した。

当日は、作製した $\text{La}_{1-x}\text{Ce}_x\text{NiO}_2$ の物性について報告する予定である。

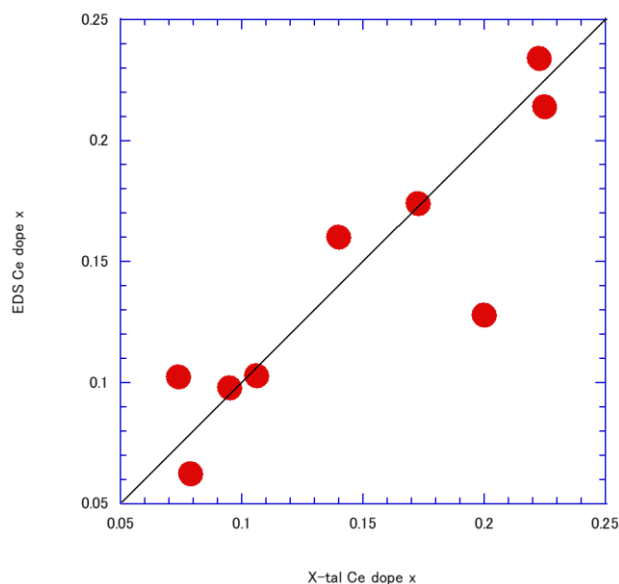


Fig1.Ce dope x by X-tal and EDS

#### Reference

[1] D. Li et al, “Superconductivity in an infinite-layer nickelate.”: Nature<sup>572</sup>, 624–627 (2019).

# Nd:YAG レーザーを用いた PLD 法によるニッケル酸化物薄膜の作製と トポケミカル還元効果

## Preparation of Nickelate Thin films by PLD Utilizing a Nd:YAG Laser and Topochemical Reduction Effects

上智大学理工<sup>1</sup>, 東北大金研<sup>2</sup>, KEC 物構研<sup>3</sup>

○(M1)森田 航太<sup>1</sup>, 山下 琉斗<sup>1</sup>, 土橋 礼奈<sup>1</sup>, 岡部 博幸<sup>2,3</sup>, 中村 惇平<sup>3</sup>, 桑原 英樹<sup>1</sup>,  
門野 良典<sup>3</sup>, 足立 匡<sup>1</sup>

Sci. and Technol., Sophia Univ.<sup>1</sup>, IMR, Tohoku Univ.<sup>2</sup>, KEC-IMSS<sup>3</sup>

°Kota Morita<sup>1</sup>, Ryuto Yamashita<sup>1</sup>, Reina Tsuchihashi<sup>1</sup>, Hirotaka Okabe<sup>2,3</sup>, Jumpei Nakamura<sup>3</sup>,  
Hideki Kuwahara<sup>1</sup>, Ryosuke Kadono<sup>3</sup>, Tadashi Adachi<sup>1</sup>

E-mail: k-morita-1s7@eagle.sophia.ac.jp

【緒言】以前、無限層構造を有するニッケル酸化物  $RE_{1-x}(\text{Ca}, \text{Sr})_x\text{NiO}_2$  ( $RE$  = 希土類)の薄膜で超伝導が観測された[1]。Ni は+1 価で  $3d^9$  の電子配置を取るなど、銅酸化物高温超伝導体との共通点がある。そこで、低エネルギーミュオンを用いてニッケル酸化物のスピン揺らぎが調べられたが、母物質とホールドーピングされて超伝導が現れる試料で磁性に変化がないなど、不明な点がある[2]。そこで本研究では、J-PARC で稼働し始めた超低速ミュオンを用いてスピン揺らぎの知見を得るため、前駆体のペロブスカイト構造  $\text{La}_{1-x}\text{Sr}_x\text{NiO}_3$  ( $x = 0, 0.2$ )の薄膜を作製し、トポケミカル還元によって無限層  $\text{La}_{1-x}\text{Sr}_x\text{NiO}_2$  ( $x = 0, 0.2$ )の合成を試みた。

【実験】 $\text{La}_{1-x}\text{Sr}_x\text{NiO}_3$  ( $x = 0, 0.2$ )の薄膜は、通常のエキシマレーザーよりも簡便な Nd:YAG レーザーの第3高調波を用いたパルスレーザー堆積(PLD)法で  $\text{SrTiO}_3$  基板上に作製した。続いて薄膜と還元剤  $\text{CaH}_2$  をパイレックス管へ真空封入したのち、電気炉で加熱して還元を行った。

【結果・考察】 Fig. 1 に、基板温度  $630^\circ\text{C}$ 、酸素分圧 20 Pa、レーザー繰返し周波数 5 Hz、レーザーエネルギー密度  $3.9 \text{ J/cm}^2$  で作製した母物質の As-grown と、 $300^\circ\text{C}$  で 80 分間還元した試料における X 線回折ピークプロファイルを示す。As-grown では単相の  $\text{LaNiO}_3$  が得られ、ラウエフリングも見られたことから高品質の薄膜が得られた。還元試料では  $\text{LaNiO}_3$  のピークは消失し、 $\text{LaNiO}_2$  のピークが出現した。電気抵抗率測定の結果、As-grown 試料は金属的な振る舞いを示したが、還元試料は低温で半導体的となった。先行研究では金属的[1]、半導体的[3]な振る舞いがともに観測されているので、より品質を向上させた薄膜を調べる必要がある。

[1] D. Li *et al.*, Nature **572**, 624 (2019).

[2] J. Fowlie *et al.*, Nat. Phys. **18**, 1043 (2022).

[3] S. Zeng *et al.*, Sci. Adv. **8**, eabl9927 (2022).

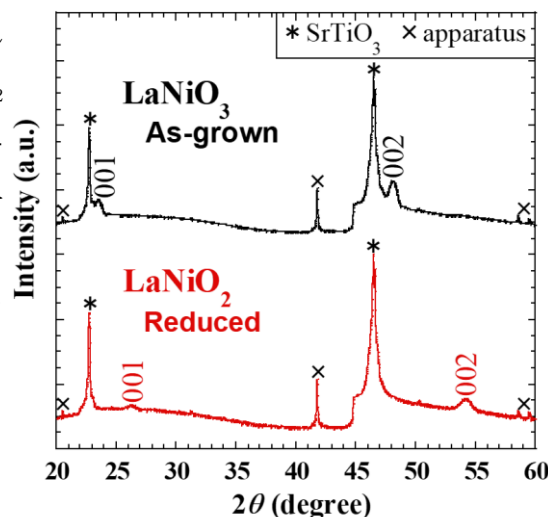


Fig. 1. X-ray diffraction pattern of  $\text{LaNiO}_3$  and  $\text{LaNiO}_2$ .



# 超伝導候補新規物質 $\text{Sr}_3\text{Ni}_2\text{O}_5\text{Cl}_2$ の高圧合成と物性評価

High-pressure synthesis and characterization of  
new compound  $\text{Sr}_3\text{Ni}_2\text{O}_5\text{Cl}_2$  that is candidate for superconductor

物材機構<sup>1</sup>, 筑波大<sup>2</sup>, KUAS<sup>3</sup>, <sup>○</sup>(D1)山根 和樹<sup>1, 2</sup>, 足立 伸太郎<sup>3</sup>, 松本 凌<sup>1</sup>, 寺嶋 健成<sup>1</sup>  
櫻井 裕也<sup>1</sup>, 高野 義彦<sup>1, 2</sup>

NIMS<sup>1</sup>, Univ. of Tsukuba<sup>2</sup>, KUAS<sup>3</sup>, <sup>○</sup>Kazuki Yamane<sup>1, 2</sup>, Shintaro Adachi<sup>3</sup>, Ryo Matsumoto<sup>1</sup>,  
Kensei Terashima<sup>1</sup>, Hiroya Sakurai<sup>1</sup>, Yoshihiko Takano<sup>1, 2</sup>

E-mail: YAMANE.Kazuki@nims.go.jp

昨年、高圧力下の Ni 酸化物  $\text{La}_3\text{Ni}_2\text{O}_{7+\delta}$  が転移温度  $T_c = 80$  K の高温超伝導体であると報告され、大きな注目を集めている[1]。常圧力下の  $\text{La}_3\text{Ni}_2\text{O}_7$  は斜方晶構造で超伝導を示さないが、20 GPa 程度の圧力で正方晶系へと構造相転移して超伝導を示すと報告された[2]。本研究では、 $\text{La}_3\text{Ni}_2\text{O}_7$  と類似の電子状態を持ち、常圧で正方晶構造となることが理論予測されている  $\text{Sr}_3\text{Ni}_2\text{O}_5\text{Cl}_2$  に着目し、その合成と物性評価を行った。

川井式マルチアンビル装置による高圧合成により、 $\text{Sr}_3\text{Ni}_2\text{O}_5\text{Cl}_2$  の多結晶試料を得た。合成した試料について、X 線回折 (XRD) パターンを測定した。また、ホウ素ドープダイヤモンドを電極としたダイヤモンドアンビル高圧セルを用いて高圧力下の電気抵抗を測定した[3]。

Fig.1 に 10 GPa, 1380 °C で得た試料の XRD パターンを示す。ほとんどの回折線が正方晶構造で指数付けされ、新規物質で目的相の  $\text{Sr}_3\text{Ni}_2\text{O}_5\text{Cl}_2$  を合成できた。Fig.2 に  $\text{Sr}_3\text{Ni}_2\text{O}_5\text{Cl}_2$  の主な圧力下における電気抵抗の温度依存性を示す。0.4 GPa から 48 GP までの圧力印加と共に抵抗が一桁ほど減少し、その後上昇に転じた。また、100 GPa を超える高圧領域まで絶縁体で超伝導を示さないことが分かった。今後は  $\text{Sr}_3\text{Ni}_2\text{O}_5\text{Cl}_2$  の結晶構造の詳細とキャリアドープの可能性について探る。

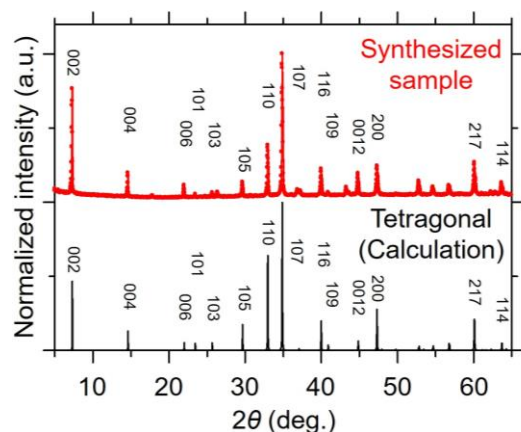


Fig.1 XRD pattern of synthesized sample.

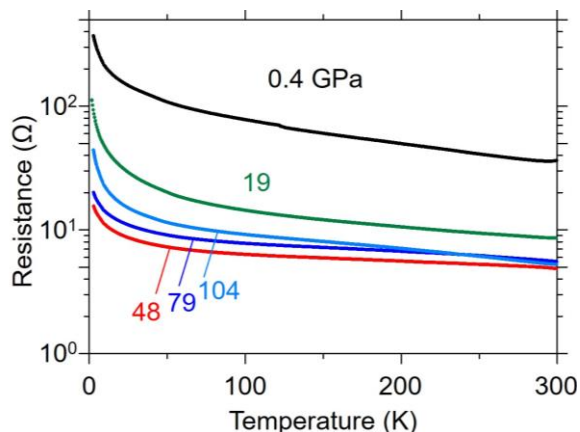


Fig.2 R-T of the sample at each pressure.

[1] H. Sun et al., Nature **621**, 493 (2023). [2] L. Wang et al., J. Am. Chem. Soc. **146**, 7506 (2024).

[3] R. Matsumoto et al., J. Appl. Phys. **56**, 05FC01 (2017).

## 高圧合成・構造解析・物性測定機能付き DAC を用いた $T_c = 20$ K 級新規超伝導体の発見

Discovery of novel superconductor with  $T_c = 20$  K using DAC with the functions of  
high-pressure synthesis, structural analysis, and physical property measurement

○松本 凌<sup>1</sup>, 山根 和樹<sup>1, 2</sup>, 寺嶋 健成<sup>1</sup>, 新名 亨<sup>3</sup>, 入船 徹男<sup>3</sup>, 櫻井 裕也<sup>1</sup>, 高野 義彦<sup>1, 2</sup>

(1. NIMS, 2. 筑波大, 3. 愛媛大)

○Ryo Matsumoto<sup>1</sup>, Kazuki Yamane<sup>1,2</sup>, Kensei Terashima<sup>1</sup>, Toru Shinmei<sup>3</sup>, Tetsuo Irifune<sup>3</sup>,

Hiroya Sakurai<sup>1</sup>, Yoshihiko Takano<sup>1,2</sup> (1. NIMS, 2. Univ. of Tsukuba, 3. Ehime Univ.)

E-mail: MATSUMOTO.Ryo@nims.go.jp

高圧合成法は、未探索の準安定領域における新規物質合成を行ううえで有効な手法であり、特に超伝導体の探索では顕著な成果を挙げている。一方で高圧準安定相の超伝導探索においては、高圧合成を行ったのち構造解析や物性測定をその場で行う必要があり、実験難易度が跳ね上がることがボトルネックとなっている。我々はこれまでに、高圧力印加装置であるダイヤモンドアンビルセル (DAC) の試料空間に、X 線を透過する導電性ダイヤモンド薄膜から成る合成用ヒーターや温度計、物性測定用電極をパターンニングすることで、高圧合成と X 線構造解析、電気抵抗測定を同一試料にて行うことができる仕組みを開発してきた[1]。この手法を用いて、第一原理計算により超伝導の候補物質と予測されていた立方晶の  $\text{Sn}_3\text{S}_4$  を初めて合成し、10 K を超える比較的高い  $T_c$  を示すことを見出した[2]。現在は同型構造におけるアニオン・カチオンサイトの置換により、類縁物質での超伝導探索と基礎物性の理解を目的に研究を進めている。

本講演では、 $\text{Sn}_3\text{S}_4$  と同型構造の  $\text{In}_{3-x}\text{S}_4$  に着目する。本物質は金属サイトの占有率に自由度があり、In が 3 価となる  $\text{In}_{2.67}\text{S}_4$  (= 整数比で  $\text{In}_2\text{S}_3$ ) の組成比で電荷中性となる。実際に過去の合成例を見ると、常圧安定相の正方晶  $\text{In}_2\text{S}_3$  を高温高圧処理することにより、立方晶の  $\text{In}_{2.67}\text{S}_4$  が得られている[3]。我々は  $\text{In}_{2.67}\text{S}_4$  の物性測定を初めて行い、 $T_c = 16$  K 前後の超伝導を示すことを前回の応物で報告した[4]。その後の検討で、試料のバッチによっては電気抵抗が 17 K 以上からわずかに減少し始めることに注目し、合成条件の最適化による  $T_c$  の向上を目指している。その結果、合成温度の上昇とともに  $T_c$  が向上し、図 1 に示すようにオンセット  $T_c$  が 20 K に到達することを発見した。構造解析の結果、焼結を行うごとに In の占有率が 1 に近づく、すなわち組成比が  $\text{In}_3\text{S}_4$  へと変化していることが示唆された。今後は高い  $T_c$  の要因解明と類縁物質におけるさらなる探索を目指す。

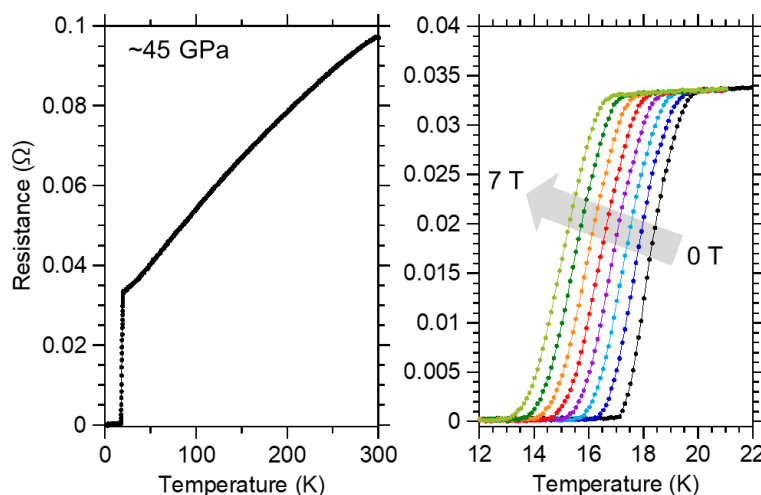


Fig. 1 Temperature dependence of resistance at around 45 GPa in  $\text{In}_{3-x}\text{S}_4$ . (a) 300-0 K, (b) 22-12 K under various magnetic fields.

- [1] R. Matsumoto et al., APL. 119, 053502 (2021). [2] R. Matsumoto et al., Inorg. Chem. 61, 4476 (2022).  
[3] S. G. Parra et al., Phys. Chem. Chem. Phys. 23, 23625 (2021). [4] 山根 他, 第 71 回応物, 24a-12P-6.



# Development of automatic synthesis system for superconducting alloys

Wei-Sheng Wang<sup>1,2</sup>, Kensei Terashima<sup>1</sup>, Yoshihiko Takano<sup>1,2</sup>

NIMS<sup>1</sup>, Univ. of Tsukuba<sup>2</sup>

Email: WANG.Wei-Sheng@nims.go.jp

The rise of materials informatics and its ability to predict material properties through computational modeling has spurred a demand for robust experimental validation. Automation using robots has emerged as a promising approach to expedite this validation process. Recent advancements in robotic systems for material synthesis have been documented in diverse areas, including liquid-phase materials[1], thin-film[2], and solid-state synthesis[3]. While robots excel at repeatable movement, achieving consistent final products remains paramount for both process optimization and obtaining materials with desired properties through Bayesian optimization techniques.

This work reports the development of an automated arc-melting system (Figure 1) for the synthesis of alloys and demonstrates its successful application in the production of several superconducting samples. The system is built upon the Robot Operating System (so-called ROS2), a flexible and scalable framework for developing robust and reliable robotic applications. ROS2 provides a structured communication architecture between various system components, including the robotic arm, vacuum chamber, arc-melting furnace, and sensors. This modular design facilitates the integration of additional components and the adaptation of the system for diverse experimental setups.

The system's basic construction is nearing completion, with successful testing of key hardware components (cooling water flow, air/Ar pressure, and electric arc control). The process begins by initiating the arc on Zr stored as an oxygen trap (Figure 2), followed by its migration towards the raw material mixture. After cooling, the material is flipped and re-melted for ensuring the reaction and the homogeneity of the product.

Despite the apparent simplicity of the process, numerous parameters can be optimized, including discharge power and distance, approach speed, arc radius, and the number of melting cycles. Leveraging the system, we have successfully synthesized several samples (Figure 3), demonstrating its potential for high-throughput and reproducible production of superconducting alloys. The developed system can be quite useful for seeking new superconducting materials with enhanced properties and broader applications.



Figure 1: Automated arc-melting system.



Figure 2: Arc-melting in automatic motion.

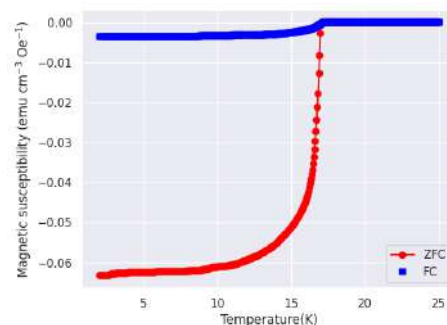


Figure 3: Magnetization data under 10 Oe, for  $Nb_3Al$  sample synthesized by the automated arc-melting system.

## References:

- [1] Benjamin Burger et al. In: *Nature* 583, 237 (2020).
- [2] Ryota Shimizu et al. In: *APL Materials* 8, 11 (2020).
- [3] Nathan J Szymanski et al. In: *Nature* 624, 86 (2023).

# (Y<sub>1-x</sub>Dy<sub>x</sub>)Ba<sub>2</sub>Cu<sub>3</sub>O<sub>y</sub> の二軸磁場配向挙動の樹脂硬化時間依存性

Resin-curing time dependence of biaxial magnetic alignment behavior for (Y<sub>1-x</sub>Dy<sub>x</sub>)Ba<sub>2</sub>Cu<sub>3</sub>O<sub>y</sub>

京都先端科学大・工: 福山風人, アリワリドビン, 足立伸太郎, 木村史子, 堀井滋

Kyoto Univ. Adv. Sci.: F. Fukuyama, W. B. Ali, S. Adachi, F. Kimura, and S. Horii

E-mail: 2024mm18@kuas.ac.jp

## 1. Introduction

To achieve the high critical current density of REBa<sub>2</sub>Cu<sub>3</sub>O<sub>y</sub> (RE123) superconductors (SCs) for practical use, bi- or tri-axial grain alignment is essential. Our group is focusing on the magnetic alignment technique to improve critical current by fabricating the thick RE123 film (> 10 μm). Biaxial alignment of RE123 grains with twinned microstructure has been achieved under the modulated rotating magnetic field of solenoidal SC magnet (SC-MRF) in an epoxy resin [1, 2]. Currently, we developed the linear drive type MRF equipment (LDT-MRF) [3]. One of the issues is development of the biaxial aligned RE123 ceramics based on the colloidal process. The time required for bi-axial magnetic alignment,  $\tau$  [s], is expressed as follows when the viscosity of the dispersed media is  $\eta$  [Pa·s],  $\Delta\chi_{ca}$  is magnetic anisotropy, and  $B$  [T] is magnetic field strength [4]:  $\tau = 6\eta\mu_0/\Delta\chi_{ca}B^2$ . Previously, we reported viscosity dependence of biaxial orientation degrees in (Y<sub>1-x</sub>Dy<sub>x</sub>)123 [5]. In principle,  $\tau$  needs to be shorter than the curing time of epoxy resins or the casting time of colloidal solution. In this study, we clarified the degrees of orientation of (Y<sub>1-x</sub>Dy<sub>x</sub>)Ba<sub>2</sub>Cu<sub>3</sub>O<sub>y</sub> [(Y<sub>1-x</sub>Dy<sub>x</sub>)123] particles under the SC-MRF and the LDT-MRF in epoxy resin with different curing times.

## 2. Experimental

(Y<sub>1-x</sub>Dy<sub>x</sub>)123 [ $x = 0, 0.02, 0.05, \text{ and } 0.1, y \sim 7$ ] polycrystals were (synthesized by the standard solid-state reaction and oxygen annealing; particle size  $\sim 10$  μm) prepared. Before the magnetic alignment, epoxy resins were pre-cured to reach the target viscosity as the initial viscosity state. (Y<sub>1-x</sub>Dy<sub>x</sub>)123 powders were mixed with pre-cured epoxy resins at weight ratio of 1:10 and aligned under SC-MRF of 0.8 T and LDT-MRF. We used three different types of epoxy resins. Resin A shows a higher initial viscosity (specification,  $\eta_{\text{init}} \sim 40$  Pa·s) and 2.7 h for curing. Resins B and C show lower initial viscosities (specification,  $\eta_{\text{init}} \sim 0.5$  Pa·s) and different curing times (17 h for B, 37 h for C). The degrees of orientation of the magnetically aligned powder samples of (Y<sub>1-x</sub>Dy<sub>x</sub>)123 were determined from (103) pole figure measurements.

## 3. Results and Discussion

Figs. 1(a) and 1(b) show (103) pole figures of the (Y<sub>0.98</sub>Dy<sub>0.02</sub>)123 ( $x = 0.02$ ) powder samples aligned under LDT-MRF, in Resin A and the pre-cured Resin

B, respectively. The pre-curing time of the pre-cured Resin B was 3 h, and its estimated viscosity is 40 Pa·s. Note that the measurement plane for the (103) pole figure is perpendicular to the direction of the static magnetic field component. For magnetically aligned (Y<sub>0.98</sub>Dy<sub>0.02</sub>)123 in Resin A, ring shape pattern was obtained, indicating that (Y<sub>0.98</sub>Dy<sub>0.02</sub>)123 in Resin A achieved high  $c$ -axis aligned and low in-plane orientation degrees. Clearly, 4-fold symmetric spots were obtained for magnetically aligned (Y<sub>0.98</sub>Dy<sub>0.02</sub>)123 in the pre-cured Resin B, indicating that (Y<sub>0.98</sub>Dy<sub>0.02</sub>)123 powders in the pre-cured Resin B was biaxial aligned. FWHM values in the rotational direction were determined using these spots. The average of FWHM values,  $\Delta\phi$ , was used as an index of the degrees of in-plane orientation. We could not determine  $\Delta\phi$  value in Fig. 1(a) because of peak broadness, while the  $\Delta\phi$  value was approximately 20 deg in Fig. 1(b). These clear differences in experimental results between Resin A and the pre-cured Resin B were obtained, suggesting that in-plane orientation degrees strongly depend on the time dependence of viscosity. In this study, we will report the change in the in-plane orientation degrees on the magnetically aligned (Y<sub>1-x</sub>Dy<sub>x</sub>)123 powder samples as functions of viscosity, curing time, and magnetic anisotropy (or  $x$ ).

## References

- [1] S. Horii *et al.*, SuST **29** (2016) 125007.
- [2] W. B. Ali *et al.*, J. Appl. Phys. **134** (2023) 163901.
- [3] S. Horii *et al.*, J. Ceram. Soc. Jpn. **126** (2018) 885.
- [4] F. Kimura and T. Kimura, Cryst. Eng. Comm. **20** (2018) 861.
- [5] F. Fukuyama *et al.*, JSAP2024, Spring Meeting, 24p-12P-7

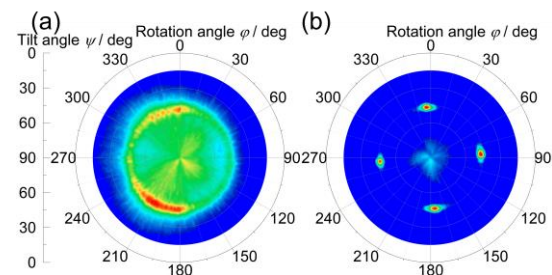


Fig. 1 (103) pole figures at  $\alpha$ -plane of the magnetically aligned powder samples of (Y<sub>0.98</sub>Dy<sub>0.02</sub>)123 under LDT-MRF in (a) Resin A ( $\eta_{\text{init}} \sim 40$  Pa·s) and (b) the pre-cured Resin B ( $\eta_{\text{init}} \sim 40$  Pa·s), respectively.

# 三軸磁気異方性を制御した $(Y_{1-x}Dy_x)124$ における三軸磁場配向度と回転変調磁場強度の関係

## Relationship between tri-axial orientation degrees and magnetic field strength of MRF on $(Y_{1-x}Dy_x)124$ with various tri-axial magnetic anisotropies

Kyoto Univ. Adv. Sci.<sup>1</sup>, CRIEPI<sup>2</sup>

◦ K.G.P.P Kahagalla<sup>1</sup>, S. Adachi<sup>1</sup>, F. Kimura<sup>1</sup>, A. Ichinose<sup>2</sup>, and S. Horii<sup>1</sup>

E-mail: 2023mm10@kuas.ac.jp

### 1. Introduction

Layered functional materials, such as thermoelectric, optical, and superconductive materials, exhibit direction-dependent of physical and mechanical properties due to their anisotropic crystal structures. However, achieving optimal performance in practical applications requires precise control over the materials microstructure and alignment. Especially in high- $T_c$  cuprate superconductors, misorientation between grains significantly reduces intergrain critical current density, necessitating tri-axial grain alignment along the  $a$ ,  $b$ , and  $c$ -axes to optimize the transport properties.

Our group has previously demonstrated a magnetic grain-orientation technique using a modulated rotating magnetic field (MRF) without relying on epitaxial growth method [1]. This method is effective for materials exhibiting tri-axial magnetic anisotropy. Advancing the magneto-scientific technique to a practical production process for RE-based cuprate superconductors requires a thorough understanding of the factors determining their magnetization axes and magnetic anisotropies. This study focused on the relationship between tri-axial orientation degrees and magnetic field strength of MRF on twin-free  $(Y_{1-x}Dy_x)Ba_2Cu_4O_8$  [ $(Y_{1-x}Dy_x)124$ ] with various tri-axial magnetic anisotropies.

### 2. Experimental Details

Single crystals of  $(Y_{1-x}Dy_x)124$  with varying nominal Dy concentration levels,  $x=0, 0.1, 0.25, 0.50, 0.75$ , and 1, were grown using the flux method [2] in ambient pressure, employing KOH as the flux medium.  $Y_2O_3$ ,  $Dy_2O_3$ ,  $BaCO_3$ , and  $CuO$  were used as starting materials in a solid-state reaction at 900 °C in air, followed by an intermediate grinding step. The resultant powder was mixed with KOH in a weight ratio of 5:6 (powder:KOH) and subjected to heat treatment at 700 °C in an  $Al_2O_3$  crucible. The crystal growth process was maintained at this temperature for 2 h, followed by a gradual cooling process at a rate of 1 °C/h. Finally, the grown crystals were thoroughly washed with distilled water several times to remove any residual flux. Scanning electron microscope images clarified the particle size and transmission electron microscopy (TEM-EDX) was used to analyze the chemical composition of synthesized samples. Pulverized  $(Y_{1-x}Dy_x)124$  microcrystals were mixed with Araldite Standard ( $\eta_{init} \sim 40$  Pas) epoxy resin in a weight ratio of 1:10 and aligned under MRFs of 1-10 T. The magnetization axes, degrees of orientation of the magnetically aligned (MA) powder samples of  $(Y_{1-x}Dy_x)124$  were determined from

XRD and (017) pole figure measurements.

### 3. Results and discussion

The XRD patterns of the MA- $(Y_{1-x}Dy_x)124$  showed the clear enhancement of (00 $l$ ), ( $h00$ ), and ( $0k0$ ) peaks at the  $\alpha$ ,  $\beta$ , and  $\gamma$  planes respectively under the MRF of 1-10 T. For  $(Y_{1-x}Dy_x)124$  ( $x=0$ ), the relationship of the magnetization axes was  $\chi_c > \chi_a > \chi_b$ , and remained unchanged with change in  $x$ .

As shown in Fig. 1(a), a ring-shaped diffraction pattern was obtained for Y124 under MRF of 1 T in (017) pole figure measurements. The results indicate that only the  $c$ -axis was aligned in above case, suggesting that the static magnetic field component alone was sufficient. In contrast, the rotating field component was not adequate. This might be due to either insufficient magnetic orientation energy or a need for a longer magnetic alignment time. The two-fold symmetric spots were observed at MRF of 10 T as shown in Fig. 1(b). High degrees of in-plane orientation with FWHM < 4° were accomplished for MA-Y124. Furthermore, even at MRF of 5 T, MA-Y124 shows high degrees of in-plane orientation with FWHM < 5°. This suggested the MRF of 5 T applied field is sufficient to achieve the desired magnetic orientation energy even at Y124. The in-plane orientation degrees were gradually increased with the increasing in  $x$ . Considering the influence of the grain size, change in the degrees of in-plane orientation on the MA- $(Y_{1-x}Dy_x)124$  will be discussed in the presentation.

### Reference

- [1] Horii, S. *et al.*, SuST, **28**, 105003 (2015).
- [2] Yamaki, M. *et al.*, Jpn. J. Appl. Phys., **51**, 0101007 (2012).

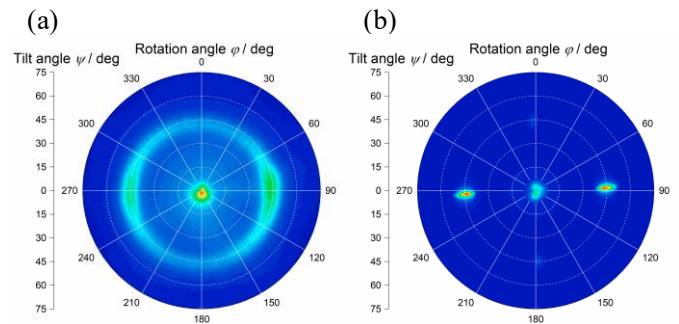


Figure 1. (017) pole figures of MA- $(Y_{1-x}Dy_x)124$  ( $x=0$ ) with (a) MRF of 1 T and (b) MRF of 10 T.  $\Psi$  and  $\phi$  indicate tilt and rotation angles, respectively.



# 試料搬送型の変調回転磁場印加による REBa<sub>2</sub>Cu<sub>3</sub>O<sub>y</sub> 磁場配向の検討

## Study of magnetic alignment in REBa<sub>2</sub>Cu<sub>3</sub>O<sub>y</sub> through sample-transport-based modulated rotating magnetic field application

京都先端科学大・工：〇足立 伸太郎, 木村 史子, 堀井 滋

Kyoto Univ. Adv. Sci (KUAS): 〇Shintaro Adachi, Fumiko Kimura, and Shigeru Horii

E-mail: adachi.shintaro@kuas.ac.jp

### Introduction

To achieve high critical current densities in both self-field and in-field conditions for high- $T_c$  cuprate superconductors like REBa<sub>2</sub>Cu<sub>3</sub>O<sub>y</sub> (RE123), it is crucial to achieve densification and orientation of a substantial number of grains. We are currently investigating magnetic alignment techniques to achieve biaxial orientation of RE123 grains, aiming to advance the practical utilization of RE123 as a superconducting wire. The advantages of magnetic alignment is not requiring highly oriented template materials and it is also a room temperature process. These characteristics of magnetic alignment create new opportunities for fabricating thicker films of RE123, a goal that is challenging to achieve using epitaxial technology.

In the magnetic alignment method, the expectation is that the easy and hard axes align perpendicular to the static magnetic field and the modulated rotating magnetic field, respectively. When the grain shape is approximately spherical, the following formula can be used to estimate the required magnetic alignment time  $\tau$  [1]:  $\tau^{-1} = \chi_a B^2 / 6\eta\mu_0$ , where  $\chi_a$  is the dimensionless difference between the magnetic susceptibility along the easy axis and that perpendicular to the easy axis,  $B$  is the magnetic flux density,  $\eta$  is the medium viscosity, and  $\mu_0$  is the vacuum permeability. Previously, achieving biaxial magnetic alignment of several RE123s required the superconducting magnet [2]. Recently, our group developed an original device that can generate a linear drive type of modulated rotating magnetic fields (LDT-MRF) using the permanent magnet arrays [3]. This magnetic alignment device is compact and has low (capital investment and operational) costs. Also, this LDT-MRF equipment had achieved a static magnetic field of 0.9 T and a rotating magnetic field of 0.8 T. Furthermore, recently, by expanding the width of magnet arrays perpendicular to the LDT direction, we have succeeded in suppressing the tilt of the sample grains in the direction of the hard magnetization axis, thereby achieving the high degrees of orientation of each grain [4-5]. To date, such research has been carried out using batch processes, but the application of this magnetic alignment technology requires a continuous process. In this study, we added a sample transport system to the LDT-MRF equipment and tested a continuous magnetic alignment process.

### Experimental method

Polycrystalline DyBa<sub>2</sub>Cu<sub>3</sub>O<sub>y</sub> (Dy123,  $y \sim 7$ ) powders (ave. particle size  $\sim 2-4 \mu\text{m}$ ) were used

as the test of magnetic alignments by using the LDT-MRF system, showing its relatively large magnetic anisotropy among the RE123 compounds [2-5]. "Araldite Standard" was used as the dispersion medium for Dy123 grains. The initial viscosity (catalog spec) of this epoxy resin is  $\eta_{\text{int}} \sim 40 \text{ Pa}\cdot\text{s}$ , and less than  $5*\eta_{\text{int}}$  even after 1 h of mixing. The time when the sample entered/escaped the magnetic field region of the LDT-MRF was defined as  $t_{\text{sta}}/t_{\text{end}}$ , respectively. The orientation state of the Dy123 grains after magnetic alignment was investigated by using the (1 0 3) pole figures.

### Results and discussion

Figures 1a and 1b show the (1 0 3) pole figure results for Sample A and Sample B, respectively. The 4-fold rotationally symmetric spots indicate the biaxial orientation of Dy123 grains with twin microstructures. In both the results for samples A and B, 4 spots and their centers of gravity were shifted in parallel downward on this paper. Such a parallel shift indicates that the grain orientation state is tilted. Specifically, the ends of the Dy123 grains closest to the magnet side were lifted and tilted as the sample escaped from the magnetic field region. The inclination of Sample B ( $\sim 10^\circ$ ) was smaller than that of Sample A ( $\sim 20^\circ$ ). Higher viscosity of the sample when it's escaped from the magnetic field, the grain tilt may be suppressed. By adjusting the magnetic anisotropy and medium viscosity of the sample to the state of the magnetic field lines created by the magnet arrays, it may be possible to obtain a continuously magnetically aligned samples. In this presentation, we will report details of the methods and results.

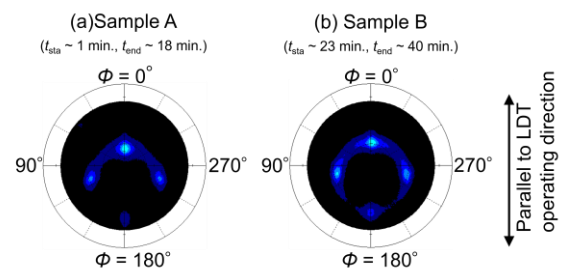


Fig. 1. Results of (1 0 3) pole figure measurements for (a) Sample A ( $t_{\text{sta}} \sim 1 \text{ min.}$ ,  $t_{\text{end}} \sim 18 \text{ min.}$ ) and (b) Sample B ( $t_{\text{sta}} \sim 23 \text{ min.}$ ,  $t_{\text{end}} = 40 \text{ min.}$ ).

### References

- [1] Kimura, *Polym. J.* **35**, 823 (2003). [2] Horii *et al.*, *SuST* **29**, 125007 (2016). [3] Horii *et al.*, *J. Cer. Soc. Jpn.* **126**, 885 (2018). [4] Ali *et al.*, *JAP* **134**, 163901 (2023). [5] Adachi *et al.*, JSAP spring MTG 2024.

# 首振り回転磁場下における $\text{REBa}_2\text{Cu}_3\text{O}_7$ 粉末( $\text{RE}=\text{Y}, \text{Er}$ )の 配向度と首振り角度の関係

Relationship between bi-axial orientation degrees and oscillation angle for  $\text{REBa}_2\text{Cu}_3\text{O}_7$  ( $\text{RE}=\text{Y}, \text{Er}$ ) powder samples aligned under oscillation type of modulated rotating magnetic fields

<sup>1</sup>京都先端科学大学・工, <sup>2</sup>京大院エネ科: °堀井滋<sup>1</sup>, 野津乃祐<sup>2</sup>, 土井俊哉<sup>2</sup>

<sup>1</sup>Kyoto Univ. Adv. Sci., <sup>2</sup>Kyoto Univ.: °S. Horii<sup>1</sup>, D. Notsu<sup>2</sup> and T. Doi<sup>2</sup>

E-mail: horii.shigeru@kuas.ac.jp

## 1. Introduction

$\text{REBa}_2\text{Cu}_3\text{O}_7$  ( $\text{RE}123$ , RE: rare-earth elements) shows critical temperature around 90 K and relatively higher critical current densities under magnetic field at 77 K. Due to the weak link at grain boundary in  $\text{RE}123$ , biaxial/triaxial grain orientation is necessary for practical use. Our group focuses on biaxial/triaxial magnetic alignment by modulated rotating magnetic field (MRF). In principle, the intermittent type MRF[1], which is typically used in our group, includes different processes of the static (SF) and rotating (RF) fields. In the present study, our group uses another type of MRF, an oscillation (OS) type MRF[2]. Fig. 1 shows a schematic of the OS type MRF and its advantages are that the OS process includes both the SF and RF components and the two components are determined by the oscillation angle ( $\theta$ ) systematically. We investigate the biaxial orientation degrees of twinned Y123 and Er123 powder samples aligned under the OS type MRF with controlling  $\theta$  and magnetic field ( $B_a$ ) systematically.

## 2. Experimental

Oxygen-postannealed Y123 ( $\chi_c > \chi_a > \chi_b$ ) and Er123 ( $\chi_b > \chi_a > \chi_c$ ) polycrystals were pulverized in a agate mortar. The powders were mixed with epoxy resin (Araldite Standard,  $\eta_{\text{mi}}=40$  Pas) in a weight ratio with powder : resin = 1:10, and were cured in the OS type MRF. As shown in Fig. 1,  $\theta$  is the maximum OS angle created by the normal direction to the  $\alpha$  plane and the horizontal  $B_a$  direction of the superconducting solinoidal electromagnet. In this study, rotation speed ( $\Omega$ ) is 5 rpm and  $\theta$  is  $1.8^\circ \sim 90^\circ$ . (103) pole figure measurement is examined to determine the biaxial orientation degree ( $F$ ) of the magnetically aligned powder samples of Y123 and Er123.

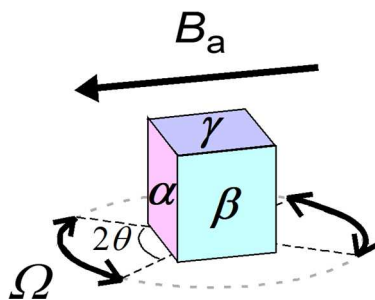


Fig. 1 Experimental configuration in oscillated rotation magnetic fields.

## 3. Results and discussion

In principle, within  $\theta < 90^\circ$ , the first easy, second easy and hard axes are aligned normal to the  $\alpha$ ,  $\beta$  and  $\gamma$  planes of Fig. 1, respectively. Fig. 2 shows relationship between  $F$  and  $\theta$  for the magnetically aligned Y123 powder samples with  $B_a = 1, 5$  and 10 T. Incidentally, the  $\gamma$  plane was used as the measurement plane for the (103) pole figure measurement in the Y123 powder samples.

The  $F$  values show  $\sim 10\%$  for 1 T, suggesting that the biaxial alignment is not achieved in a whole region of  $\theta$ . For 5 and 10 T,  $F \sim 10\%$  emerges only in a lower  $\theta$  region, while  $F$  increases with the increase in  $\theta$ . The increase in  $\theta$  means the increase in the RF component. It is strongly suggested from Fig. 2 that sufficient RF component for achieving magnetic separation of the  $a$ -axis and  $b$ -axis is obtained by using wider oscillation angles even in 5 and 10 T.

In this presentation, the results in Er123 are also shown, and their relationships between  $F$  and  $\theta$  will be discussed from the theoretical viewpoints.

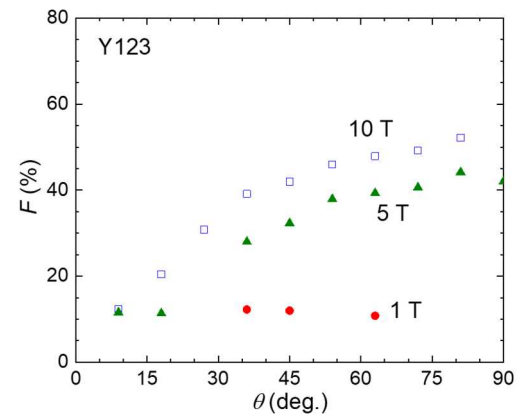


Fig. 2 Relationship between  $F$  and  $\theta$  for the magnetically aligned Y123 powder samples.

## Acknowledgments

This work was partly supported by JST-ASTEP (Stage I) and KAKENHI (17H03235).

## References

- [1] Horii *et al.*, SuST 29 (2016) 125007.
- [2] Yamaki, Horii *et al.*, Phys. Procedia 58 (2014) 62.